Clay Minerals (2021), **56**, 156–167
doi:10.1180/clm.2021.29

CAMBRIDGE UNIVERSITY PRESS

Article

In situ synthesis of zeolites by geopolymerization with NaOH/KOH mixed solution and their potential application for Cd(II) immobilization in paddy soil

Di Wu, Yi Huang*, Guqing Xiao, Xuan Li, Xia Yao, Zixuan Deng and Rui Tan
School of Materials and Chemical Engineering, Hunan City University, Yiyang 413002, China

Abstract

Geopolymers can be transformed into zeolites under certain synthesis conditions. However, zeolite formation is not frequently reported in KOH-activated geopolymers. This study attempted to explore zeolite synthesis through geopolymerization for a curing time of 24 h using mixed NaOH/KOH alkaline solution as an activator, and then applying the geopolymer-supported zeolites to immobilize Cd(II) in paddy soil. The $K_2O/M_2O–H_2O/SiO_2$ and $K_2O/M_2O–OH^-/SiO_2$ binary zeolite crystallization phase diagrams were obtained. Zeolite A, faujasite and sodalite formed at lower K_2O/M_2O molar ratios (0–0.2), ferrierite formation was favoured at a K_2O/M_2O molar ratio of 0.2–0.4 and zeolite K-I and zeolite F-K (both K-zeolites) were observed at a K_2O/M_2O molar ratio of 0.6. The geopolymer-supported zeolites had micropores and mesopores and specific surface area values of 44.2–74.8 $m^2\ g^{-1}$. The material displayed a considerable Cd(II) immobilization efficiency (55.6–58.7% at 4–6 wt.% addition of zeolite).

Keywords: available potassium, Cd(II) immobilization, geopolymer, *in situ* zeolite synthesis, NaOH/KOH mixed alkaline solution

(Received 30 April 2021; revised 9 September 2021; Accepted Manuscript online: 30 September 2021; Associate Editor: Lawrence Warr)

Geopolymers are alkali-activated (alumino)silicate cementitious materials that have been used in construction materials, fire-resistant materials and heavy-metal adsorption and solidification (Davidovits, 1991; Temuujin *et al.*, 2009; Shaqour *et al.*, 2017; Ng *et al.*, 2018; Esaifan *et al.*, 2019; Rasaki *et al.*, 2019; Padilla *et al.*, 2020). The typical manufacturing process of geopolymers involves the addition of an alkaline activator (a mixed solution of sodium or potassium hydroxide and sodium or potassium silicate) to a poorly crystallized or amorphous aluminosilicate material such as fly ash or metakaolin (MKn) and subsequent mixing and curing at a moderate temperature (20–95°C). Geopolymers present a three-dimensional network structure that is composed of SiO_4 and AlO_4 tetrahedral units linked together by bridge oxygen atoms. The empirical formula for geopolymers is as follows:

$$M_n(-(SiO_2)_z-AlO_2-)_n\cdot wH_2O \quad (1)$$

where M is a cation such as potassium (K) or sodium (Na), n is the degree of polycondensation, z is 1–3 and w is the amount of binding water (van Deventer *et al.*, 2007). According to the z value, geopolymers are classified as poly(sialate) (PS), poly(sialate-siloxo) (PSS) or poly(sialate-disiloxo) (PSDS) (Davidovits, 2008).

Na-PS presents a sodalite cage structure formed by connected single four- and six-membered rings (Davidovits, 2008), from which hydroxysodalite, faujasite and zeolite A are built (Buchwald *et al.*, 2011). Therefore, geopolymers may be regarded as zeolite precursors, whereby hydroxysodalite, faujasite and zeolite A can form in Na-geopolymers with lower Si/Al ratios (Takeda *et al.*, 2012; Duan *et al.*, 2015). In recent years, the *in situ* preparation of zeolites by geopolymerization has received much attention because it is a simple and low-cost process compared with the traditional hydrothermal method (Ge *et al.*, 2014; Liguori *et al.*, 2019). However, K-geopolymers are less suitable for zeolite formation because K favours the formation of less ordered structures, favouring the formation of geopolymeric networks, which are amorphous (Duxson *et al.*, 2007a; Hu *et al.*, 2017). Therefore, K-zeolite formation has been reported rarely in previous studies on geopolymers. de Moraes Pinheiro *et al.* (2018) observed that zeolite K-I ($K_2Al_2Si_2O_8\cdot3.8H_2O$) and potassium gismondine ($K_2Al_2Si_2O_8\cdot3H_2O$) formed in KOH-activated geopolymers after curing at 65°C for 7 days using blast furnace slag as the starting material. Zeolite K-I was also observed in clay-based geopolymers activated with 5 M KOH solution after curing for 4 months, while K-chabazite formed after such curing for 1 year (El Hafid & Hajjaji, 2015). In addition, zeolite K, zeolite V, zeolite X and zeolite F were identified in KOH-activated geopolymers immersed in NaCl solutions after ageing for 28 days (Fu *et al.*, 2020). From the aforementioned studies, it is concluded that a long curing time is necessary for geopolymer transformation into K-zeolite.

Cadmium (Cd) is ranked as the seventh most toxic heavy metal among environmental pollutants by the Agency for Toxic Substance and Disease Registry (ASTR 2017). Industrial development and intensive agriculture release large amounts of Cd, resulting in the Cd contamination of soil. Cd-contaminated soils are a global environmental concern, causing damage not

*E-mail: jeremyme@163.com
Cite this article: Wu D, Huang Y, Xiao G, Li X, Yao X, Deng Z, Tan R (2021). *In situ* synthesis of zeolites by geopolymerization with NaOH/KOH mixed solution and their potential application for Cd(II) immobilization in paddy soil. *Clay Minerals* **56**, 156–167. https://doi.org/10.1180/clm.2021.29

only to human health and ecology, but there are also significant economic implications with respect to reclamation and restoration costs (Semenzin *et al.*, 2007). In China, Cd is the most widespread heavy-metal pollutant in soils(Hu *et al.*, 2020); urgent remediation is required. The technology of *in situ* immobilization with amendments remediates soils contaminated by heavy metals (Amanullah *et al.*, 2015). Zeolite is a valuable amendment for heavy-metal immobilization in soils because of its large specific surface area and ion-exchange capacity (Ansari Mahabadi *et al.*, 2007; Shi *et al.*, 2009; Zhao *et al.*, 2020). In addition, zeolite is also a potential soil conditioner that can improve soil fertility, infiltration and hydraulic conductivity and control soil pH (Szerement *et al.*, 2021). K-zeolite is more suitable than Na-zeolite for heavy-metal immobilization in paddy soils because it may serve as an effective slow-release potassium fertilizer (Zwingmann *et al.*, 2011; Najafi-Ghiri *et al.* 2014); Na^+ is not considered to be an essential nutrient and its excess adversely affects the growth of plants (Hasegawa *et al.*, 2020; Zhu, 2001). Investigation of the *in situ* synthesis of K-zeolite by geopolymerization with a short curing time and its application to remedy Cd-contaminated paddy soils was therefore deemed worthwhile.

In geopolymer and zeolite synthesis, the OH^- ion acts as a reaction catalyst and the alkaline metal cation acts as a structure-forming element (Duxson *et al.*, 2007b). Suzuki *et al.* (2009) studied the cooperative effect of Na^+ and K^+ in forming a framework of ferrierite zeolite and concluded that K^+ contributed to the formation of the building units of ferrierite, while Na^+ contributed to the final crystallization so as to order the building units in a (Na, K)-system. Based on this observation, the present work attempts to synthesize zeolites using a KOH/NaOH mixed alkaline solution as an activation agent and a curing time of 24 h for geopolymerization. Metakaolin was selected as the starting material because of its high reactivity and purity compared to other materials such as fly ash, slag and natural clay (Zhang *et al.*, 2012; Autef *et al.*, 2013). The factors that influence zeolite formation were investigated using X-ray diffraction (XRD) analysis, and then $K_2O/M_2O–H_2O/SiO_2$ and $K_2O/M_2O–OH^-/SiO_2$ binary zeolite crystallization phase diagrams were obtained. Finally, the immobilization potential of Cd(II) in paddy soil of the respective geopolymer-supported zeolites was evaluated.

Materials and methods

In situ *synthesis of zeolites transformed from geopolymer precursors*

The MKn raw material was purchased from JingYang Kaolin Company, Shanxi Province, China. The chemical composition of MKn as determined by X-ray fluorescence (XRF; PANalytical B.V. Company Axios Advanced, The Netherlands) is listed in Table 1. The cadmium nitrate ($Cd(NO_3)_2$), sodium hydroxide (NaOH) and potassium hydroxide (KOH) used in this study were analytical reagent (AR) grade and were purchased from Sinopharm Chemical Reagent Co., Ltd (China). NaOH and KOH were dissolved in deionized water to obtain NaOH/KOH mixed-alkaline solutions.

Deionized water, MKn and the mixed-alkaline solution were mixed thoroughly with a NJ-160A mechanical blender (Wuxi Jianyi Experiment Co., Ltd, China), producing a homogeneous paste. The molar composition of the paste was: $xK_2O{:}yNa_2O{:}SiO_2{:}0.39Al_2O_3{:}zH_2O$ (the Al_2O_3/SiO_2 molar ratio of MKn was 0.39 as calculated from Table 1). Then the paste was poured into 20 mm × 20 mm × 20 mm steel cubic moulds and cured at 80°C at a relative humidity of 95 ± 5% for 24 h. Lastly, the samples were demoulded and ground to powders below 300 mesh with a pestle and mortar for characterization.

Table 1. Chemical composition of MKn as determined by XRF analysis.

Component	SiO_2	Al_2O_3	Fe_2O_3	TiO_2	P_2O_5	K_2O	CaO	Na_2O	LOI
wt.%	58.56	38.74	0.59	0.68	0.24	0.13	0.33	0.32	0.45

LOI = loss on ignition.

Sample characterization

The mineralogical composition of the synthesized materials and MKn was determined by XRD using a Bruker AXS D8 Advance diffractometer (Germany) with a graphite monochromator, using Cu-*K*α radiation, 40 kV and 40 mA in the range 5–90°2θ with a scanning speed of 2° min^{-1}. The morphology of the samples was characterized with a SU8010 field emission scanning electron microscope (FESEM; Hitachi Company, Japan) at an acceleration voltage of 2 kV. Uncoated samples were used. Fourier-transform infrared (FTIR) spectra of the synthetic products and MKn were collected with resolution of 2 cm^{-1}, in the spectral range of 400–4000 cm^{-1} on a Thermo Nicolet Nexus spectrometer (USA), using the KBr pellet technique. The specific surface area and pore volume of the synthesized samples were determined with a Micromeritics ASAP 2020 instrument by N_2 adsorption/desorption at 77 K on materials degassed at 200°C for 10 h prior to analysis. The micropore (pore size <2 nm) volume (V_{mic}) and micropore area (S_{mic}) were calculated using the t-plot method. The mesopore (2 nm < pore size < 50 nm) volume (V_{mes}) was calculated with the Barrett–Joyner–Halenda (BJH) method. The specific surface area (S_{BET}) values were determined using the Brunauer–Emmet–Teller (BET) method.

Construction of binary zeolite crystallization phase diagrams

Based on the XRD traces, the $K_2O/M_2O–H_2O/SiO_2$ binary zeolite crystallization phase diagram (namely the zeolite types as functions of the K_2O/M_2O and H_2O/SiO_2 molar ratios) and the $K_2O/M_2O–OH^-/SiO_2$ binary zeolite crystallization phase diagram (namely the zeolite types as functions of the K_2O/M_2O and OH^-/SiO_2 molar ratios) were constructed.

Immobilization of Cd(II) in paddy soil

The uncontaminated paddy soil was collected from 20 cm of topsoil in the suburb of Yiyang, Hunan Province, using a five-point sampling mode, then mixed and air dried. The <2 mm fraction was artificially polluted with aqueous solutions of Cd(II) in the form of Cd $(NO_3)_2$. The soil samples were mixed thoroughly and cultivated under natural conditions for 20 days, maintaining a water content of 70%. The dosage of Cd(II) was 5 mg kg^{-1}.

Soil pH was determined using a PHS-3C pH meter with a soil/water ratio of 1:2.5 (w/v). The available potassium in the soil was extracted with ammonium acetate (pH = 7) based on the Chinese Standard NY T 889-2004 and analysed by inductively coupled plasma optical emission spectrometry (ICP-OES; SPECTRO Analytical Instruments GmbH, USA). Analyses were performed in triplicate and the results were expressed as the average values with standard deviation (σ).

https://doi.org/10.1180/clm.2021.29 Published online by Cambridge University Press

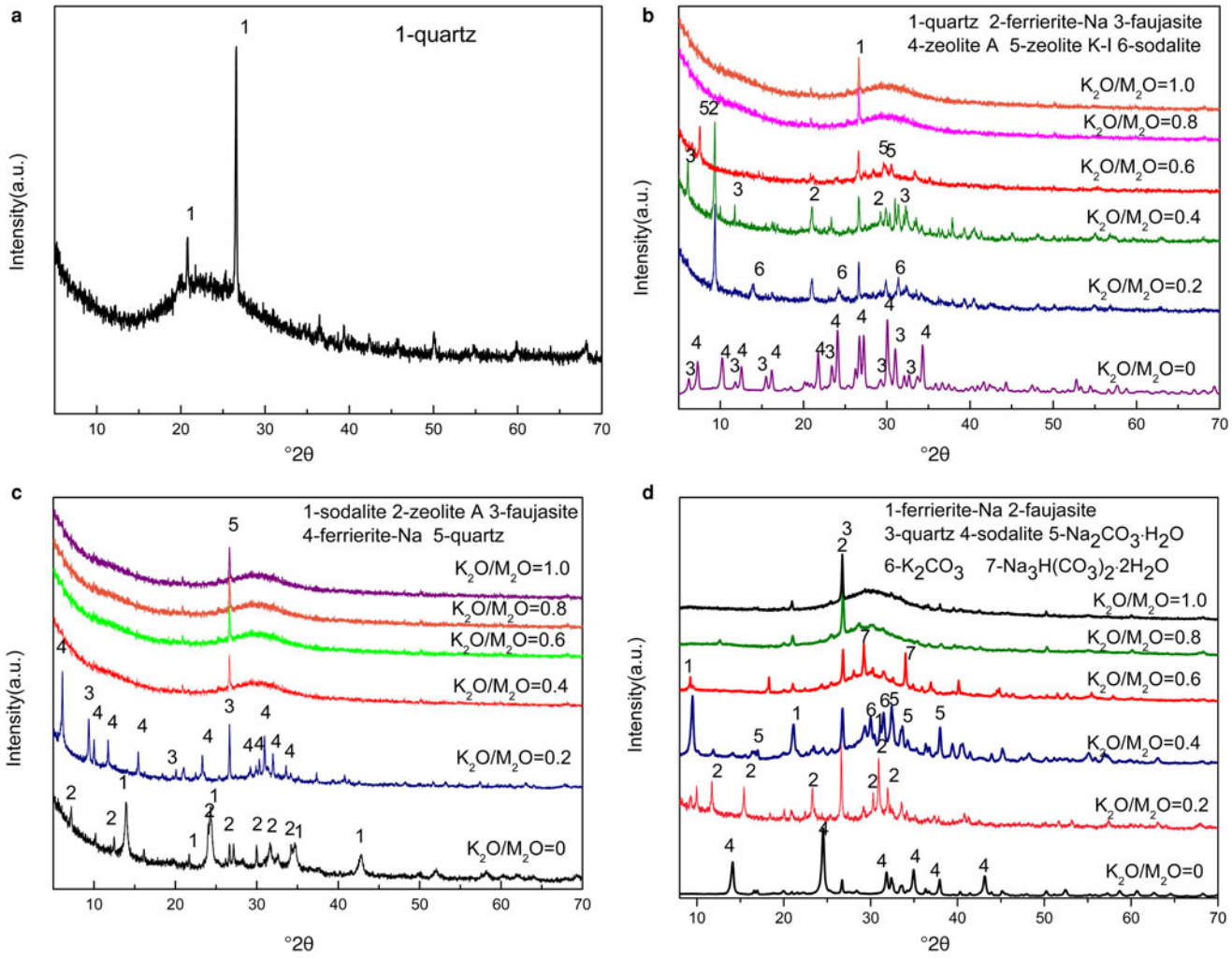

Fig. 1. XRD traces of (a) MKn raw material and geopolymer samples with H_2O/SiO_2 ratios of (b) 5.5, (c) 7.4 and (d) 9.3 at the OH^-/SiO_2 ratio of 1.36.

The representative geopolymer-supported zeolites were added to the contaminated soil in dosages of 2, 4, 6 and 8 wt.% and then were thoroughly mixed. The amended soil was adjusted to 70% of the water content and incubated for 2 days at room temperature. Then the bioavailable Cd content of the soil was determined according to the Chinese standard HJ804-2016. Briefly, the soil sample and diethylenetriaminepentaacetic acid (DTPA) extraction solution were added into the extraction bottle at a liquid/solid ratio of 2:1. The suspension was agitated on a HY-2A thermostatic water bath oscillator (Shanghai Lichen Instrument Co., Ltd, China) at 20 ± 2°C for 2 h at 160–200 rpm and was filtered through a medium-speed quantitative filter paper. The filtrate was analysed for bioavailable Cd concentration using ICP-OES. Three replicates were obtained for each sample and the means with standard deviation (σ) were reported.

The immobilization efficiency (R) of Cd(II) was calculated from Equation 2:

$$R = 1 - \frac{c_e}{c_i} m \quad (2)$$

where c_i and c_e (mg kg^{-1}) represent the average bioavailable Cd contents in the soil before and after immobilization, respectively.

Results and discussion

K_2O/M_2O–H_2O/SiO_2 binary zeolite crystallization phase diagram

Figure 1 shows the XRD traces of the MKn raw material and the synthesized samples with the chemical composition of $xK_2O{:}yNa_2O{:}SiO_2{:}0.39Al_2O_3{:}zH_2O$ ($x/(x+y)$ varying from 0 to 1, z varying from 5.5 to 9.3 and $x+y=1.36$). The K_2O/M_2O ($x/(x+y)$)–H_2O/SiO_2 (z) binary zeolite crystallization phase diagram with a fixed M_2O/SiO_2 molar ratio ($x+y$) of 1.36 is shown in Fig. 2. The detailed mixture proportions of samples 1–18 (Fig. 2) are listed in Table 2, and the structures, secondary building units (SBUs) and chemical formulae of the zeolites formed in samples 1–18 (Fig. 2) are summarized in Table 3.

The MKn raw material is mainly amorphous, as is indicated by the hump at ~23°2θ (Duxson *et al.*, 2007a), with trace quartz impurity. In Na-geopolymers ($K_2O/M_2O = 0$), the formation of sodalite (PDF#81-0705), zeolite A (PDF#39-0222) and faujasite (PDF#28-1036) with a sodalite cage as a composite building unit was favoured. Sodalite tended to occur in samples with greater H_2O/SiO_2 as opposed to lower H_2O/SiO_2, which favoured zeolite A formation.

https://doi.org/10.1180/clm.2021.29 Published online by Cambridge University Press

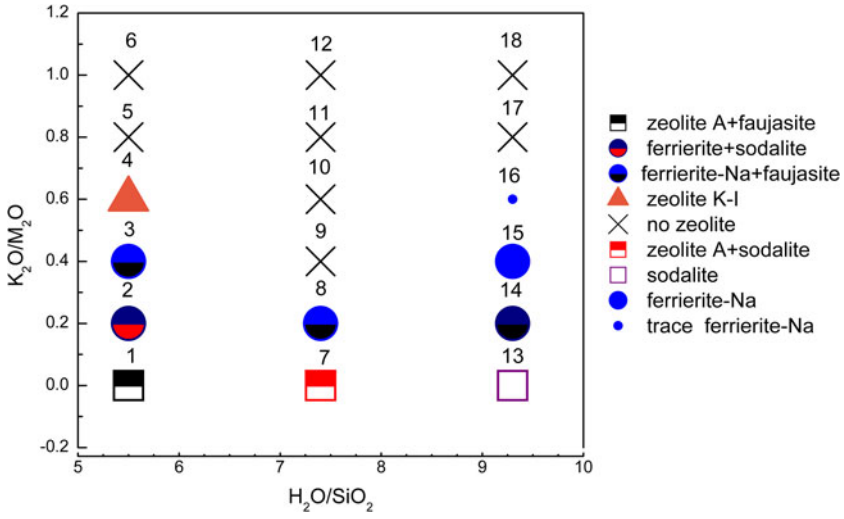

Fig. 2. K_2O/M_2O–H_2O/SiO_2 binary zeolite crystallization phase diagram of geopolymer samples activated with NaOH/KOH mixed alkaline solution. The sample numbers are marked at the top of each sample symbol.

Table 2. Detailed mixture proportions of the various samples.

Sample no.	KOH/solid (mass ratio)	NaOH/solid (mass ratio)	Water/solid (mass ratio)
1	0	0.53	1.0
2	0.15	0.43	1.0
3	0.30	0.32	1.0
4	0.45	0.21	1.0
5	0.60	0.11	1.0
6	0.75	0	1.0
7	0	0.53	1.3
8	0.15	0.43	1.3
9	0.30	0.32	1.3
10	0.45	0.21	1.3
11	0.60	0.11	1.3
12	0.75	0	1.3
13	0	0.53	1.7
14	0.15	0.43	1.7
15	0.30	0.32	1.7
16	0.45	0.21	1.7
17	0.60	0.11	1.7
18	0.75	0	1.7
19	0	0.43	1.3
20	0.12	0.34	1.3
21	0.24	0.26	1.3
22	0.36	0.17	1.3
23	0.48	0.085	1.3
24	0.60	0	1.3
25	0	0.64	1.3
26	0.18	0.51	1.3
27	0.36	0.38	1.3
28	0.54	0.26	1.3
29	0.72	0.13	1.3
30	0.90	0	1.3

Ferrierite-Na (PDF#43-0557), which is fundamentally constructed from five-membered rings, appeared or became the dominant zeolite type over the K_2O/M_2O range of 0.2–0.4. In the Na-aluminosilicate system, the crystallization area for ferrierite is limited to a very narrow region (Suzuki *et al.*, 2009); therefore, it was only occasionally detected in Na-geopolymers.

The zeolite K-I (PDF#18-0988), a K-zeolite that was discovered in the 1950s (Sherman, 1977), was only found in sample 4 ($K_2O/M_2O = 0.6$, $H_2O/SiO_2 = 5.5$). Zeolite K-I probably formed

Table 3. Zeolite structures formed in the geopolymers activated with the NaOH/KOH mixed solution (www.izastructure.org/databases).

Zeolite structure	Zeolite	SBU	SBU image	Chemical formula
LTA	Zeolite A	4–4		$Na_{96}Al_{96}Si_{96}O_{384}{\cdot}216H_2O$
FAU	Faujasite	6–6	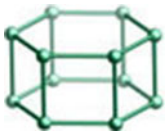	$Na_2Al_2Si_{2.4}O_{8.8}{\cdot}6H_2O$
SOD	Sodalite	6	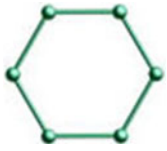	$Na_8Al_6Si_6O_{24}(OH)_2{\cdot}2H_2O$
FER	Ferrierite-Na	5–1		$Na_2Al_2Si_{2.71}O_{9.42}{\cdot}4.39H_2O$
EDI	Zeolite F-K	4 = 1		$KAlSiO_4{\cdot}1.5H_2O$
BPH	Zeolite K-I[1]	6×1		$K_2Al_2Si_2O_8{\cdot}3.8H_2O$

[1]Zeolite K-I is identical to Linde Q (Sherman, 1977).

https://doi.org/10.1180/clm.2021.29 Published online by Cambridge University Press

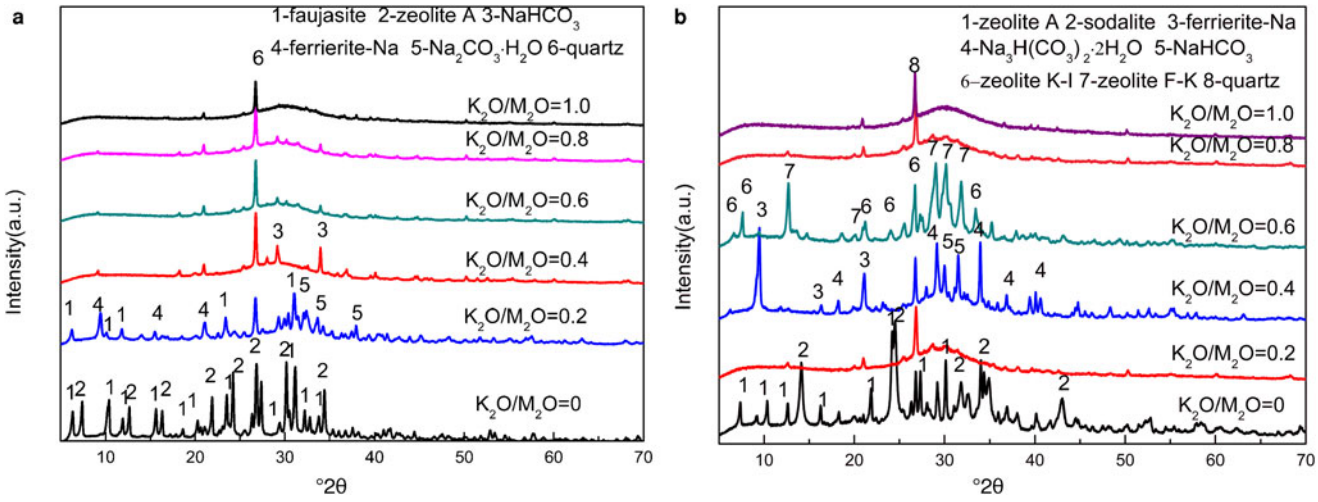

Fig. 3. XRD traces of geopolymer samples with OH^-/SiO_2 ratios of (a) 1.09 and (b) 1.63 at the H_2O/SiO_2 ratio of 7.4.

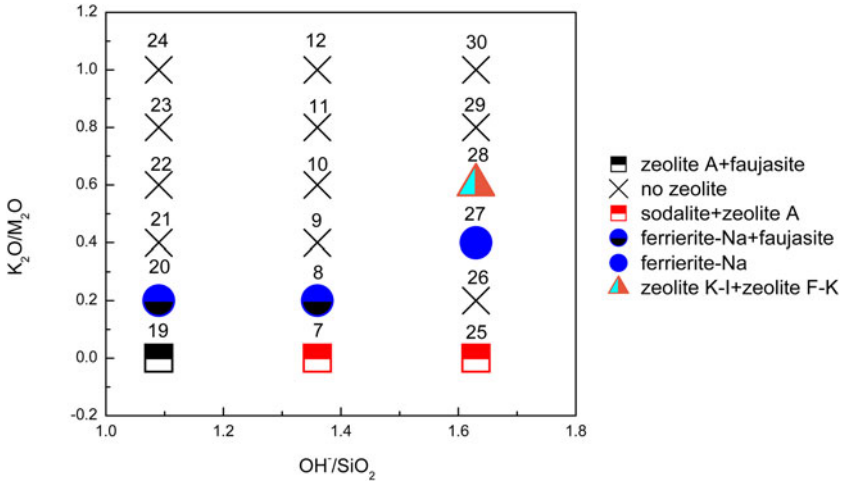

Fig. 4. K_2O/M_2O–OH^-/SiO_2 binary zeolite crystallization phase diagram of geopolymer samples activated with NaOH/KOH mixed-alkaline solution. The sample numbers are marked at the top of each sample symbol.

due to the greater alkaline concentration of the solution (i.e. a lower H_2O/SiO_2 ratio at a constant OH^-/SiO_2 ratio).

When the K_2O/M_2O ratio exceeded 0.6, almost no zeolite could be observed and a hump at ~28°2θ ascribed to the amorphous geopolymer appeared (Duxson *et al.*, 2007a). This confirmed that in the K_2O–Na_2O–SiO_2–Al_2O_3–H_2O geopolymer system, an excessive K^+ content prevented zeolites from crystallizing because the large ionic size of K^+ favours the formation of large silica oligomers (Duxson *et al.*, 2007b), hindering the movement and reorganization of ions to form crystals (Fu *et al.*, 2020). This also suggested that Na^+ plays a significant role in ordering the SBUs.

Finally, the appearance of $Na_2CO_3·H_2O$ (PDF#72-0578), K_2CO_3 (PDF#87-0730) and $Na_3H(CO_3)_2·2H_2O$ (PDF#75-1195) in some samples should be attributed to the reaction between the excessive NaOH or KOH and CO_2 in air.

K_2O/M_2O–OH^-/SiO_2 binary zeolite crystallization phase diagram

Figure 3 shows the XRD traces of the synthesized samples with chemical composition xK_2O:yNa_2O:SiO_2:$0.39Al_2O_3$:zH_2O ($x/(x+y)$ = 0–1, $x+y$ = 1.09 or 1.63 and z = 7.4). The K_2O/M_2O ($x/(x+y)$)–OH^-/SiO_2 ($x+y$) binary zeolite crystallization phase diagram with a fixed H_2O/SiO_2 molar ratio (z) of 7.4 is shown in Fig. 4. The detailed mixture proportions of samples 19–30 (Fig. 4) are listed in Table 2, and the structures, SBUs and chemical formulae of the zeolites formed in samples 19–30 (Fig. 4) are summarized in Table 3.

In Na-geopolymers, sodalite, zeolite A and faujasite remained the dominant zeolites. Zeolite A appeared over the complete OH^-/SiO_2 ratio range. By contrast, sodalite preferentially formed at higher OH^-/SiO_2 ratios, whereas lower OH^-/SiO_2 ratios favoured the presence of faujasite. This was in agreement with previous published studies (Król *et al.*, 2018; Rózek *et al.*, 2018).

Ferrierite was still detected in geopolymer samples synthesized using solutions with a K_2O/M_2O ratio range of 0.2–0.4. At the K_2O/M_2O ratio of 0.6, zeolites (zeolite K-I and zeolite F-K (PDF#38-0216)) were observed only in the samples with the highest OH^-/SiO_2 ratio (= 1.63), confirming that the synthesis of these two zeolites takes place at greater alkali concentrations. Zeolite F-K is also a K-zeolite that was discovered in the 1950s (Sherman, 1977). The chemical composition of zeolite K-I and zeolite F-K is the same as kaliophilite ($KAlSiO_4$) except for the amount of zeolitic water, verifying that K-PS has a kaliophilite-like structure (Davidovits, 2008). Zeolites occur essentially as alteration products

https://doi.org/10.1180/clm.2021.29 Published online by Cambridge University Press

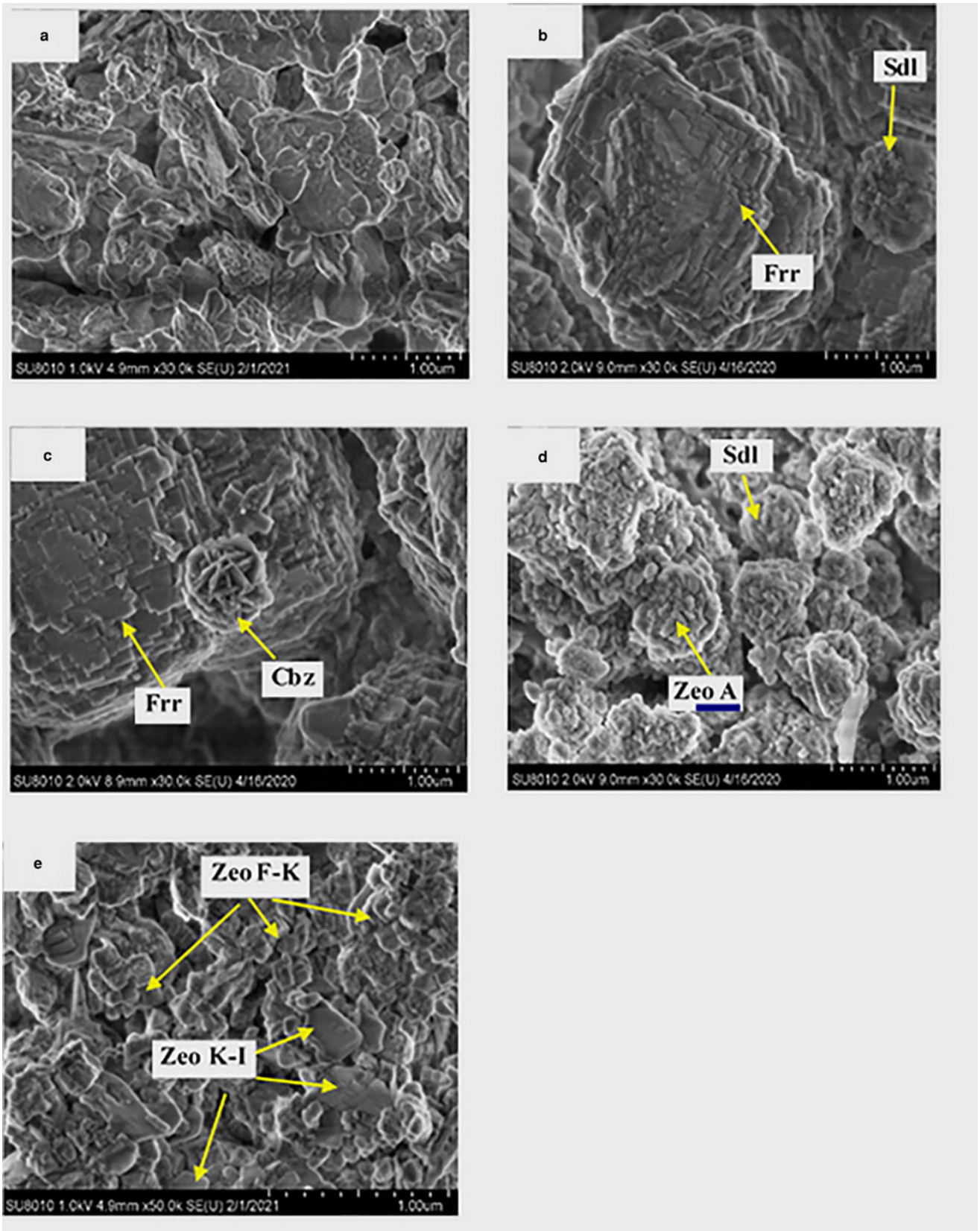

Fig. 5. FESEM images of representative samples: (a) sample 22, (b) sample 2, (c) sample 8, (d) sample 25, (e) sample 28. Cbz = chabazite; Frr = ferrierite; Sdl = sodalite; Zeo A = zeolite A; Zeo F-K = zeolite F-K; Zeo K-I = zeolite K-I.

https://doi.org/10.1180/clm.2021.29 Published online by Cambridge University Press

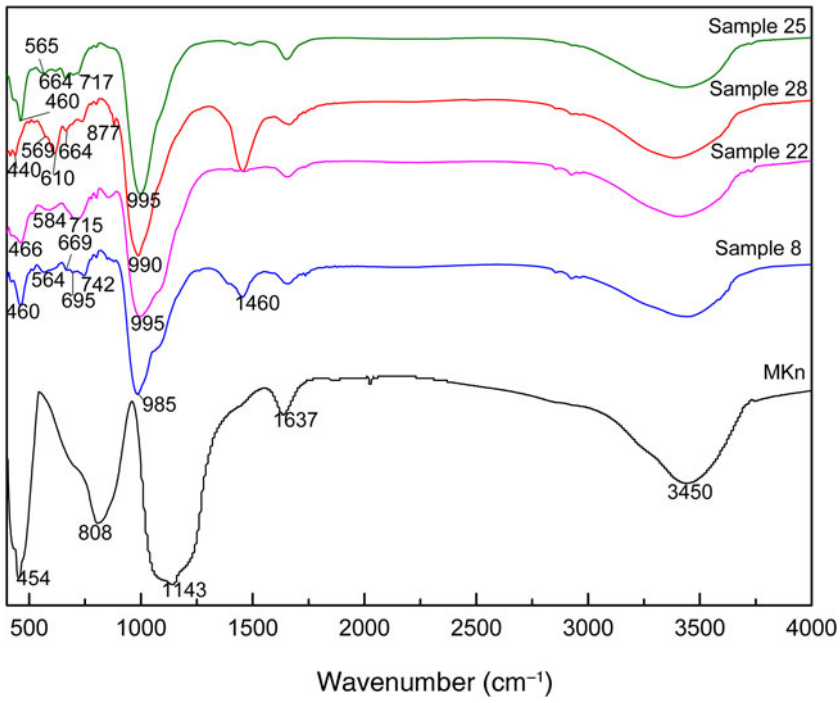

Fig. 6. FTIR spectra of the MKn raw material and representative geopolymer samples.

of (Na, Ca)-aluminosilicates such as nepheline and plagioclase. K-aluminosilicates (kalsilite, leucite, sanidine) are more resistant to hydrothermal degradation than other species, resulting in abundant K-zeolites in nature (Davidovits, 2008). In the present study, a novel *in situ* synthesis method for K-zeolites by geopolymerization is proposed.

No zeolites were observed in the samples with K_2O/M_2O ratios >0.6. Carbonates including $Na_2CO_3{\cdot}H_2O$, $NaHCO_3$ (PDF#74-1203) and $Na_3H(CO_3)_2{\cdot}2H_2O$ were also identified in some of the end products.

FESEM analysis of representative samples

The FESEM images of representative samples (samples 2, 8, 22, 25 and 28) are shown in Fig. 5. Sample 22, which was the only sample without zeolite formation, mainly consisted of geopolymers with a disordered morphology (Fig. 5a). In sample 2, the ferrierite particles ~2 μm in diameter consisted of stacked rectangular crystals, and the sodalite appeared to have a ball-like morphology (Lee *et al.*, 2016) with an average diameter of ~1 μm (Fig. 5b). The ferrierite crystals in sample 8 had a similar morphology to that of sample 2; walnut-shaped chabazite (Duxson *et al.*, 2007b) was occasionally found on the surface of ferrierite particles (Fig. 5c). Zeolite A in sample 25 displays a grape-like morphology consisting of clusters of agglomerated block crystals with an average diameter of ~100 nm (He *et al.*, 2013), and the sodalite has a similar morphology and an average diameter similar to that of sample 2. In sample 28, the cubic-shaped crystal probably belongs to zeolite F-K and the plate-like crystal is possibly zeolite K-I (Sherman, 1977).

FTIR analysis of representative samples

Figure 6 shows the FITR spectra of MKn and representative samples (samples 8, 22, 25 and 28). For MKn, the band at 808 cm^{-1} is a characteristic peak of Al(VI)–O bonds, and that at 1143 cm^{-1} is attributed to the Si–O–*T* (*T* = Si or Al) asymmetric stretching vibration (Temuujin *et al.*, 2009). After geopolymerization, the former band disappeared and the latter band shifted to ~990 cm^{-1} due to the transformation of Al(VI) or Al(V) present in MKn to Al(IV) (Duxson *et al.*, 2007a). The bands at 3450 and 1637 cm^{-1} were ascribed to O–H stretching and bending modes of adsorbed molecular water (Liguoria *et al.*, 2019), and the band at 1460 cm^{-1} was due to the O–C–O stretching vibration (Liu *et al.*, 2016). In addition, the bands in the range 400–900 cm^{-1} were different for the various samples. In sample 22 (without zeolite formation), the bands at 466, 584 and 715 cm^{-1} were related to the Al–O/Si–O bending, Si–O–Al bending and Si–O–Si/Si–O–Al symmetric stretching vibrations, respectively, of geopolymer (Liu *et al.*, 2016). The broad band at ~565 cm^{-1} was assigned to the vibration of six-membered rings and double four-membered rings of zeolite A and sodalite (Rózek *et al.*, 2019) in sample 25 ($K_2O/M_2O = 0$). The bands at 460 and 664 cm^{-1} are also characteristic of these two zeolites (Huang *et al.*, 2012; Yao *et al.*, 2009). In sample 8 ($K_2O/M_2O = 0.2$), the overlap of bands at 563 cm^{-1} assigned to the five-membered ring vibration of ferrierite (Jansen *et al.*, 1984) and at 565 cm^{-1} assigned to the double six-membered ring vibration of faujasite (Liu *et al.*, 2016) resulted in a broad band at ~564 cm^{-1}. Small amounts of K^+ in the starting geopolymer gel might prevent the formation of zeolite A or sodalite with four-membered rings as SBUs and facilitate the formation of ferrierite with five-membered rings as SBUs (Isobe *et al.*, 2012). In addition, the band at 460 cm^{-1} is due to the Al–O/Si–O bending vibration of faujasite and ferrierite, and the weak bands at 669 and 695 cm^{-1} correspond to TO_4 (*T*= Si or Al) tetrahedral symmetric stretch vibrations of faujasite and ferrierite, respectively (Jansen *et al.*, 1984; Liu *et al.*, 2016). For sample 28 ($K_2O/M_2O = 0.6$), the bands at 569 and 610 cm^{-1} were assigned to the zigzag eight-membered ring vibration of zeolite K-F (Wong *et al.*, 2017), and the bands at 440, 664 and 877 cm^{-1} might be the characteristic peaks of zeolite K-I (Zhang *et al.*, 2007).

https://doi.org/10.1180/clm.2021.29 Published online by Cambridge University Press

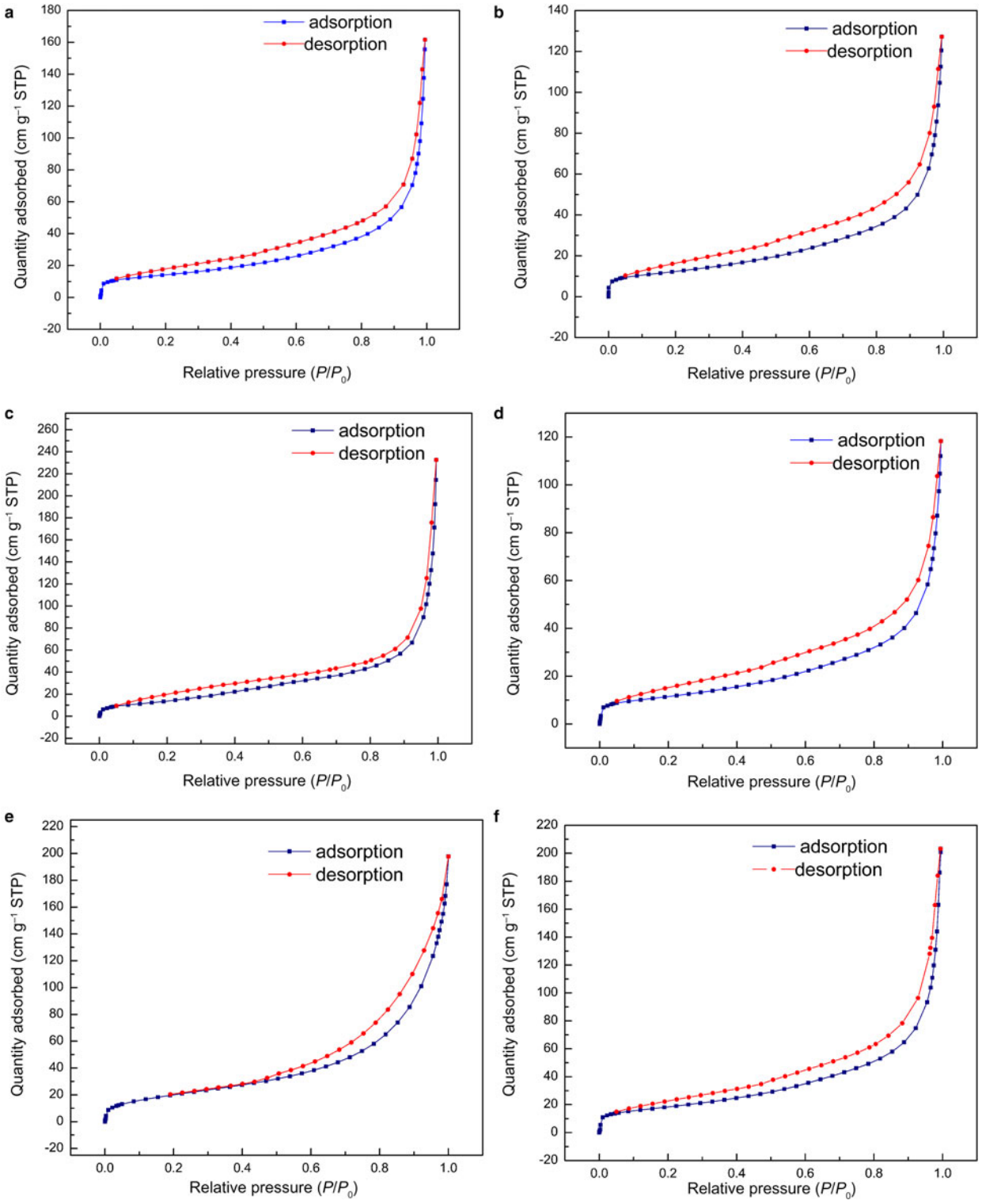

Fig. 7. N_2 adsorption–desorption isotherms at 77 K of (a) sample 2, (b) sample 7, (c) sample 8, (d) sample 22, (e) sample 25 and (f) sample 28. STP = standard temperature and pressure.

Porosity and specific surface area analysis of representative samples

The N_2 adsorption–desorption isotherms of the representative samples are illustrated in Fig. 7 and the specific surface areas and pore volumes of the samples are summarized in Table 4. All analysed samples showed type IV isotherms based on the classification of the International Union of Pure and Applied Chemistry (IUPAC) (Ariharan *et al.*, 2017). At low relative pressure ($P/P_0 < 0.05$) a small and quick uptake was observed, indicating the existence of small micropores characteristic of zeolites (Ariharan *et al.*, 2017). An H_3-type hysteresis loop in the

https://doi.org/10.1180/clm.2021.29 Published online by Cambridge University Press

Table 4. Specific surface areas and pore volumes of the representative samples. V_{mic} and V_{mes} are micropore and mesopore volumes, respectively, and S_{mic} is the specific surface area due to micropores. S_{BET} is the total specific surface area.

Sample no.	V_{mic} ($cm^3\ g^{-1}$)	V_{mes} ($cm^3\ g^{-1}$)	S_{mic} ($m^2\ g^{-1}$)	S_{BET} ($m^2\ g^{-1}$)
2	0.0020	0.238	14.4	50.1
7	0.0001	0.184	10.6	44.2
8	0.0120	0.329	13.6	53.6
22	0.0001	0.172	10.5	41.1
25	0.0004	0.314	16.2	65.7
28	0.0088	0.266	20.4	74.4

IUPAC classification occurring in all samples is considered characteristic of mesoporous materials that may be produced by interparticle spaces (Lee *et al.*, 2016). In general, these samples demonstrate the coexistence of micropores and mesopores. These conclusions correspond well with the results listed in Table 4. The samples containing zeolites (samples 2, 7, 8, 25 and 28) had greater S_{BET} values (44.2–74.8 $m^2\ g^{-1}$) and pore volumes than the sample without zeolite formation (sample 22), which is in good agreement with previous studies on the *in situ* synthesis of zeolites by geopolymerization (He *et al.*, 2013; Tang *et al.*, 2015, 2016). Note, however, that sample 22 has a similar pore volume and specific surface area to sample 7, which supports the idea that amorphous geopolymers contain nanocrystalline zeolites that cannot be detected by XRD (Provis *et al.*, 2005).

Cd(II) immobilization potential of geopolymer-supported zeolites in paddy soil

Two representative samples (samples 8 and 28) were selected to immobilize Cd(II) in paddy soil. The samples were fully washed to remove excess Na^+ and K^+ before being added to the soil. The immobilization efficiencies calculated using Equation 2 for soils containing various amounts of the two representative samples are shown in Fig. 8. The Cd(II) immobilization efficiency increased with the dosage until it reached 6 wt.% for sample 8 or 4 wt.% for sample 28. For greater dosages, the efficiency remained constant for sample 8 or increased slightly for sample 28. The maximum immobilization efficiency reached 58.7% for sample 28, being slightly greater than that for sample 8 (55.6%). This may be attributed to the greater S_{BET} of sample 28 (see Table 4). Compared with the Cd immobilization efficiency evaluated by extractable Cd content in soils using other sorbents (see Table 5), the performance of geopolymer-supported zeolites in this study was better than that of natural minerals (e.g. zeolite, bentonite and sepiolite) and similar to that of biochar.

Some previous studies (Shaha *et al.*, 2012; Hamid *et al.*, 2020; Liu *et al.*, 2021) indicated that an increase of soil pH with alkaline materials may be associated with improved Cd precipitation and adsorption. In this study, the pH value increased with the addition of greater amounts of geopolymer due to the alkaline nature of the material added (Fig. 9). However, the Cd(II) immobilization efficiency was not related to the pH value over the geopolymer-supported zeolite dosage range of 4–8 wt.%. This may be due to the competitive adsorption of excessive free Na^+ and K^+ at greater zeolite dosages, which decreased the Cd(II) adsorption capacity of the soil (Zhou *et al.*, 2003). Furthermore, K^+ has been reported to have a more negative effect on the Cd adsorption capacity of soils (Ren *et al.*, 2020), which may explain the slight lower immobilization efficiency of sample 28 at a dosage of 6–8 wt.%.

Figure 10 shows the available potassium content in the soil at various dosages of geopolymer-supported zeolites. A nearly linear increase of available potassium content with increasing dosage in the soil was observed; sample 28 with a greater K_2O/M_2O ratio provided more potassium to the soil. Therefore, this material is especially suitable for application in potassium-deficient soils. However, whether such a large potassium content is beneficial to the growth of crops should be examined in detail in a future study.

Summary and conclusions

(Na, K)-zeolites were synthesized from geopolymer precursor phases with NaOH/KOH mixed-alkaline activator solutions and were used to develop $K_2O/M_2O–H_2O/SiO_2$ and $K_2O/M_2O–OH^-/SiO_2$ binary zeolite crystallization phase diagrams. Zeolite

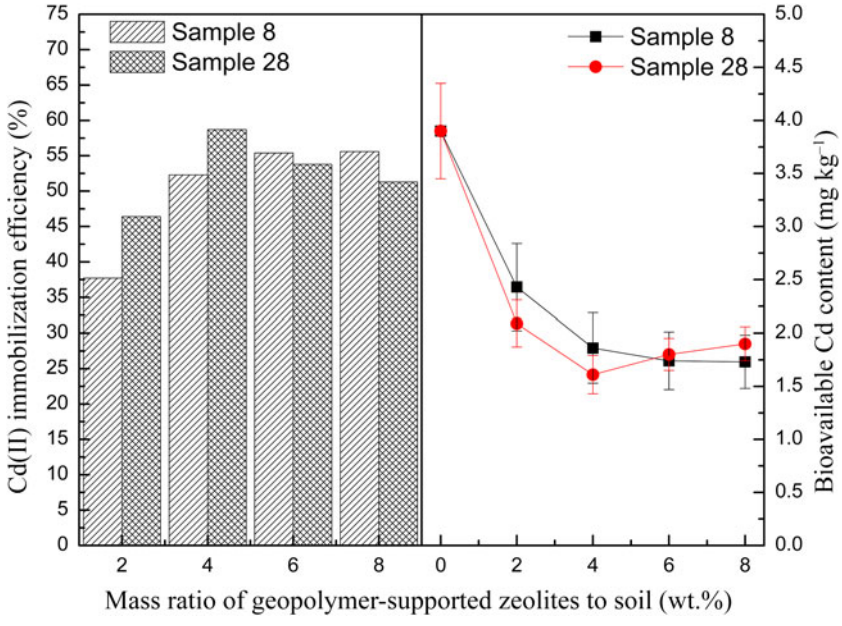

Fig. 8. Immobilization efficiency of Cd(II) and bioavailable Cd content in paddy soil for representative samples activated with a NaOH/KOH mixed solution.

https://doi.org/10.1180/clm.2021.29 Published online by Cambridge University Press

Table 5. Reported results on the immobilization capacity of various adsorbents of Cd^{2+}.

Sample	Cd immobilization efficiency (%)	Dosage (wt.%)	Ref.
Sample 28	58.7	4	This study
Sample 8	55.6	6	This study
Fe-Zeolite	29.8	1	Shahmoradi *et al.* (2020)
Fe-Bentonite	16.2	1	Shahmoradi *et al.* (2020)
Biochar	35.8	1	Liu *et al.* (2021)
Composite amendments	38.3	1	Hamid *et al.* (2020)
Biochar	60.0–70.0	6	Xu *et al.* (2020)
Modified montmorillonite	65.9	5	Wang *et al.* (2020)
Modified sepiolite	48.46	4	Xie *et al.* (2020)
Modified biochar	40.0–60.0	6	Zhang *et al.* (2020)

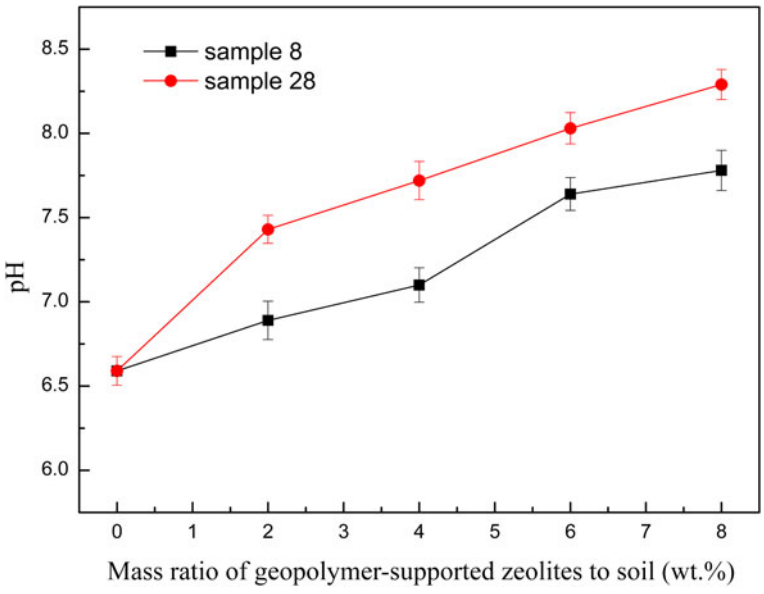

Fig. 9. The relationship between the pH value of the soil and increasing contents of two representative geopolymer samples.

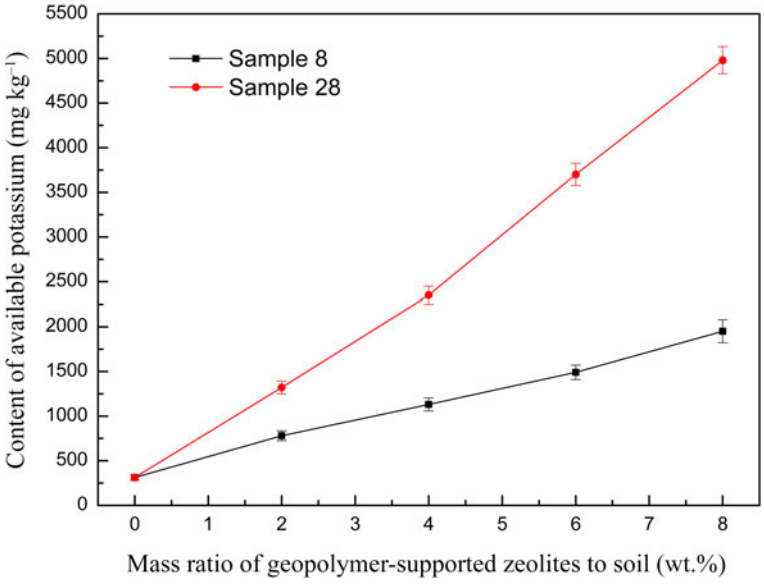

Fig. 10. The relationship between the available potassium content of the soil and the dosage of two representative geopolymer samples.

https://doi.org/10.1180/clm.2021.29 Published online by Cambridge University Press

A, faujasite and sodalite tended to form over the K_2O/M_2O ratio range of 0–0.2, ferrierite could be observed at the K_2O/M_2O ratio range of 0.2–0.4 and zeolite K-I and zeolite F-K (two K-zeolites) appeared only in samples with a K_2O/M_2O ratio of 0.6 at greater alkali concentrations. When the K_2O/M_2O ratio exceeded 0.6, zeolite formation was hindered. It is assumed that the cooperative effect of K^+ and Na^+ favours zeolite crystallization in geopolymer samples activated with NaOH/KOH mixed alkaline solutions. Most of the zeolites in the geopolymer material demonstrated an agglomerated appearance under FESEM. The samples containing zeolites were characterized by the coexistence of mesopores and micropores and a S_{BET} in the range of 44.2–74.8 m^2 g^{-1}. *In situ* synthesis by geopolymerization with NaOH/KOH mixed alkaline solution as the activator provides a novel method for zeolite preparation, especially for K-based zeolites.

The geopolymer-supported zeolites show considerable efficiency at immobilizing Cd(II) from a paddy soil (55.6–58.7% at 4–6 wt.% dosage). The pH and the available potassium content of the soil increased with increasing dosage. However, the influence of this on crop growth needs to be studied further through plant-growing experiments.

Financial support. The authors acknowledge support from the Natural Science Foundation of Hunan Province, China (Grant No. 2020JJ4157), the Undergraduate Training Program for Innovation and Entrepreneurship of Hunan Province (Grant No. S202011527032) and the Natural Science Foundation of China (Grant No. 51678225).

References

Amanullah M., Ping W., Li R.H. & Zhang Z.Q. (2015) Immobilization of lead and cadmium in contaminated soil using amendments: a review. *Pedosphere*, **25**, 555–568.

Ansari Mahabadi A., Hajabbasi M.A., Khademi H. & Kazemian H. (2007) Soil cadmium stabilization using an Iranian natural zeolite. *Geoderma*, **137**, 388–393.

Ariharan A., Viswanathan B. & Nandhakumar V. (2017) Nitrogen doped graphene as potential material for hydrogen storage. *Graphene*, **6**, 41–60.

ASTR (2017) *Toxicological Profile for Cadmium*. Department of Health and Human Services, Public Health Service, Centers for Disease Control and Prevention, Atlanta, GA, USA, 46 pp.

Autef A., Joussein E., Poulesquen A., Gasgnier G., Pronier S., Sobrados I. *et al.* (2013) Influence of metakaolin purities on potassium geopolymer formulation: the existence of several networks. *Journal of Colloid and Interface Science*, **48**, 43–53.

Buchwald A., Zellmann H.D. & Kaps C. (2011) Condensation of aluminosilicate gels model system for geopolymer binders. *Journal of Non-Crystalline Solids*, **357**, 1376–1382.

Davidovits J. (1991) Geopolymers: inorganic polymeric new materials. *Journal of Thermal Analysis*, **37**, 1633–1656.

Davidovits J. (ed.) (2008) *Geopolymer Chemistry and Applications*. Geopolymer Institute, Saint-Quentin, France, 58 pp.

de Moraes Pinheiro S.M., Font A., Soriano L., Tashima M.M., Monzó J., Borrachero M.V. & Payá J. (2018) Olive-stone biomass ash (OBA): an alternative alkaline source for the blast furnace slag activation. *Construction and Building Materials*, **178**, 327–338.

Duan J.X., Li J. & Lu Z.Y. (2015) One-step facile synthesis of bulk zeolite A through metakaolin-based geopolymer gel. *Journal of Porous Materials*, **22**, 1519–1526.

Duxson P., Fernández-Jiménez A., Provis J.L., Lukey G.C., Palomo A. & van Deventer J.S.J. (2007a) Geopolymer technology: the current state of the art. *Journal of Materials Science*, **42**, 2917–2933.

Duxson P., Mallicoat S.W., Lukey G.C., Kriven W.M. & van Deventer J.S.J. (2007b) The effect of alkali and Si/Al ratio on the development of mechanical properties of metakaolin-based geopolymers. *Colloids and Surfaces A*, **292**, 8–20.

El Hafid K. & Hajjaji M. (2015) Effects of the experimental factors on the microstructure and the properties of cured alkali-activated heated clay. *Applied Clay Science*, **116–117**, 202–210.

Esaifan M., Warr L.N., Grathoff G., Meyer T., Schafmeister M.T., Kruth A. & Testrich H. (2019) Synthesis of hydroxy-sodalite/cancrinite zeolites from calcite-bearing kaolin for the removal of heavy metal ions in aqueous media. *Minerals*, **9**, 484.

Fu C.Q., Ye H.L., Zhu K.Q., Fang D.M. & Zhou J.B. (2020) Alkali cation effects on chloride binding of alkali-activated fly ash and metakaolin geopolymers. *Cement and Concrete Composites*, **104**, 103721.

Ge Y.Y., Tang Q., Cui X.M., He Y. & Zhang J. (2014) Preparation of large-sized analcime single crystals using the geopolymer-gels-conversion (GGC) method. *Materials Letters*, **13**, 515–518.

Hamid Y., Tang L., Hussain B., Usman M., Gurajala H.K., Rashid M.S. *et al.* (2020) Efficiency of lime, biochar, Fe containing biochar and composite amendments for Cd and Pb immobilization in a co-contaminated alluvial soil. *Environmental Pollution*, **257**, 113609.

Hasegawa P.M., Bressan R.A. & Pardo J.M. (2020) The dawn of plant salt tolerance genetics. *Trends in Plant Science*, **5**, 317–319.

He Y., Cui X.M., Liu X.D., Wang Y.P., Zhang J. & Liu K. (2013) Preparation of self-supporting NaA zeolite membranes using geopolymers. *Journal of Membrance Science*, **447**, 67–72.

Hu N., Bernsmeier D., Grathoff G.H. & Warr L.N. (2017) The influence of alkali activator type, curing temperature and gibbsite on the geopolymerization of an interstratified illite–smectite rich clay from Friedland. *Applied Clay Science*, **135**, 386–393.

Huang Y., Han M.F. & Yi R.M. (2012) Microstructure and properties of fly ash-based geopolymeric material with 5A zeolite as a filler. *Construction and Building Materials*, **33**, 84–89.

Hu B.F., Shao S.H., Ni H., Fu Z.Y., Hu L.S., Zhou Y. *et al.* (2020) Current status, spatial features, health risks, and potential driving factors of soil heavy metal pollution in China at province level. *Environmental Pollution*, **266**, 114961.

Isobe M., Moteki T., Tanahashi S., Kimura R., Kamimura Y., Itabashi K. & Okubo T. (2012) Plate-like precursors formed in crystallization process of ferrierite from (Na, K)-aluminosilicate system. *Microporous and Mesoporous Materials*, **158**, 204–208.

Jansen J.C., van der Gaag F.J. & van Bekkum H. (1984) Identification of ZSM-type and other 5-ring containing zeolites by i.r. spectroscopy. *Zeolites*, **8**, 369–372.

Król M., Rózek P., & Rożek P. (2018) The effect of calcination temperature on metakaolin structure for the synthesis of zeolites. *Clay Minerals*, **53**, 657–663.

Lee N.K., Khalid H.R. & Lee H.K. (2016) Synthesis of mesoporous geopolymers containing zeolite phases by a hydrothermal treatment. *Microporous and Mesoporous Materials*, **229**, 22–30.

Liguori B., Aprea P., Roviello G. & Ferone C. (2019) Self-supporting zeolites by geopolymer gel conversion (GGC). *Microporous and Mesoporous Materials*, **286**, 125–132.

Liu Y., Yan C.J., Zhang Z.H., Wang H.Q., Zhou S. & Zhou W. (2016) A comparative study on fly ash, geopolymer and faujasite block for Pb removal from aqueous solution. *Fuel*, **185**, 181–189.

Liu B.B., He Z.L., Liu R.L., Monrenegro A.C., Ellis M., Li Q.F. & Baligar V.C. (2021) Comparative effectiveness of activated dolomite phosphate rock and biochar for immobilizing cadmium and lead in soils. *Chemosphere*, **266**, 129202.

Najafi-Ghiri M. (2014) Effects of zeolite and vermicompost applications on potassium release from calcareous soils. *Soil and Water Research*, **9**, 31–37.

Ng C., Alengaram U.J., Wong L.S., Mo K.H., Jumaat M.Z. & Ramesh S. (2018) A review on microstructural study and compressive strength of geopolymer mortar, paste and concrete. *Construction and Building Materials*, **186**, 851–860.

Padilla J., Guzman A., Molina D. & Poveda-Jaramillo J.C. (2020) Structural transformation of kaolin as an active matrix for the *in situ* synthesis of zeolite Y. *Clay Minerals*, **55**, 293–302.

Provis J.L., Lukey G.C. & van Deventer J.S.J. (2005) Do geopolymers actually contain nanocrystalline zeolites? A reexamination of existing results. *Chemistry of Materials*, **17**, 3075–3085.

https://doi.org/10.1180/clm.2021.29 Published online by Cambridge University Press

Rasaki S.A., Zhang B.X., Guarecuco R., Tiju T. & Yang M.H. (2019) Geopolymer for use in heavy metals adsorption, and advanced oxidative processes: a critical review. *Journal of Cleaner Products*, **213**, 42–58.

Ren B.Z., Wu Y., Deng D.P., Tang X.F. & Li H.T. (2020) Effect of multiple factors on the adsorption of Cd in an alluvial soil from Xiba, China. *Journal of Contaminant Hydrology*, **232**, 103605.

Rózek P., Król M. & Mozgawa W. (2018) Spectroscopic studies of fly ash-based geopolymers. *Spectrochimica Acta Part A: Molecular and Biomolecular Spectroscopy*, **198**, 283–289.

Rózek P., Król M. & Mozgawa W. (2019) Geopolymer-zeolite composites: a review. *Journal of Cleaner Products*, **230**, 557–579.

Semenzin E., Critto A., Carlon C., Rutgers M. & Marcomini A. (2007) Development of a site-specific ecological risk assessment for contaminated sites: part II. A multi-criteria based system for the selection of bioavailability assessment tools. *Science of the Total Environment*, **379**, 34–45.

Semenzin E., Szatanik-Kloc A., Jarosz R., Bajda T. & Mierzwa-Hersztek M. (2021) Contemporary applications of natural and synthetic zeolites from fly ash in agriculture and environmental protection. *Journal of Cleaner Products*, **311**, 127461.

Shaha S.C., Abul Kashem M. & Osman T.K. (2012) Effect of lime and farmyard manure on the concentration of cadmium in water spinach (*Ipomoea aquatica*). *ISRN Agronomy*, **2012**, 719432.

Shahmoradi S., Mohmmad M.A. & Hajabbasi A. (2020) Efficiency of Fe-zeolite and Fe-bentonite on co-stabilization of As, Cd and Pb in contaminated soil. *International Journal of Environmental Monitoring and Analysis*, **8**, 45–49.

Shaqour F., Ismeik M. & Esaifan M. (2017) Alkali activation of natural clay using a $Ca(OH)_2/Na_2CO_3$ alkaline mixture. *Clay Minerals*, **52,** 485–496.

Sherman J.D. (1977) Identification and characterization of zeolites synthesized in the K_2O–Al_2O_3–SiO_2–H_2O system. *Molecular Sieves – II*, **3**, 30–42.

Shi W.Y., Shao H.B., Li H., Shao M.A. & Du S. (2009) Progress in the remediation of hazardous heavy metal-polluted soils by natural zeolite. *Journal of Hazardous Materials*, **170**, 1–6.

Suzuki Y., Wakihara T., Itabashi K., Ogura M.T. & Okubo (2009) Cooperative effect of sodium and potassium cations on synthesis of ferrierite. *Topics in Catalysis*, **52**, 67–74.

Takeda H., Hashimoto S. & Iwata T. (2012) Fabrication of bulk materials with zeolite from coal fly ash. *Journal of Material Cycles and Waste Management*, **14**, 403–410.

Tang Q., Ge Y.Y. & Wang K.T. (2015) Preparation of porous P-type zeolite spheres with suspension solidification method. *Materials Letters*, **161**, 558–560.

Tang Q., He Y. & Wang Y.P. (2016) Study on synthesis and characterization of ZSM-20 zeolites from metakaolin-based geopolymers. *Applied Clay Science*, **129**, 102–107.

Temuujin J., Minjigma A. & Rickard W. (2009) Preparation of metakaolin based geopolymer coatings on metal substrates as thermal barriers. *Applied Clay Science*, **46**, 265–270.

van Deventer J.S.J., Provis J.L. & Duxson P. (2007) Reaction mechanisms in the geopolymeric conversion of inorganic waste to useful products. *Journal of Hazardous Materials*, **139**, 587–598.

Wang L.W., Li X.R., Tsang D.C.W., Jin F. & Hou D.Y. (2020) Green remediation of Cd and Hg contaminated soil using humic acid modified montmorillonite: immobilization performance under accelerated ageing conditions. *Journal of Hazardous Materials*, **387**, 122005.

Wong S.F., Awala H., Vincente A., Retoux R., Ling T.C., Mintova S. *et al.* (2017) K-F zeolite nanocrystals synthesized from organic-template-free precursor mixture. *Microporous and Mesoporous Materials*, **249**, 105–110.

Xie S., Wang L., Xu Y.M., Lin D.S., Sun Y.B. & Zhen S.N. (2020) Performance and mechanisms of immobilization remediation for Cd contaminated water and soil by hydroxy ferric combined acid-base modified sepiolite (HyFe/ABsep). *Science of the Total Environment*, **740**, 140009.

Xu C.B., Zhao J.W., Yang W.J., He L., Wei W.X., Tan X. *et al.* (2020) Evaluation of biochar pyrolyzed from kitchen waste, corn straw, and peanut hulls on immobilization of Pb and Cd in contaminated soil. *Environmental Pollution*, **261**, 114113.

Yao Z.T., Li H.Y., Xia M.S., Ye Y. & Zhang L. (2009) Hydrothermal synthesis of sodalite from coal fly ash and its property characterization. *Chinese Journal of Nonferrous Metals*, **19**, 366–371.

Zhang H.Y., Zhao Y.C. & Liu C.Q. (2007) A study on physicochemical characteristics of fly ash from MSW incineration. *Shanghai Environmental Science*, **26**, 2–7.

Zhang Y.J., Sheng L., Wang C.Y. & Xu D.L. (2012) Microstructural and strength evolutions of geopolymer composite reinforced by resin exposed to elevated temperature. *Journal of Non-Crystalline Solids*, **358**, 620–624.

Zhang H., Shao J.A., Zhang S.H., Zhang X. & Chen H.P. (2020) Effect of phosphorus-modified biochars on immobilization of Cu (II), Cd (II), and As (V) in paddy soil. *Journal of Hazardous Materials*, **390**, 121349.

Zhao H., Huang X., Liu F., Hu X., Zhao X., Wang L. *et al.* (2020) A two-year field study of using a new material for remediation of cadmium contaminated paddy soil. *Environmental Pollution*, **263**, 114614.

Zhou X.Z., Xu J.M., Zhao A.Z. & Ji G.L. (2003) Effect of ionic strength and pH on interaction between Cu^{2+} and variable charge soils. *Acta Pedologica Sinica*, **40**, 845–851.

Zhu J.K. (2001) Plant salt tolerance. *Trends in Plant Science*, **6**, 66–71.

Zwingmann N., Mackinnon I. & Gilkes R.J. (2011) Use of a zeolite synthesized from alkali treated kaolin as a K fertiliser: glasshouse experiments on leaching and uptake of K by wheat plants in sandy soil. *Applied Clay Science*, **53**, 684–690.

https://doi.org/10.1180/clm.2021.29 Published online by Cambridge University Press